Proc. Indian Acad. Sci. (Earth Planet. Sci.), Vol. 102, No. 2, June 1993, pp. 329–350.


# Global spectra of energy and enstrophy and their fluxes during July 1979

S S DESAI and S K MISHRA*

Indian Institute of Tropical Meteorology, Pune 411 008, India
*National Centre for Medium Range Weather Forecasting, Mausam Bhavan, Lodi Road, New Delhi 110003, India

MS received 27 July 1992; revised 19 January 1993

**Abstract.** Transient and stationary spectra of kinetic energy ($KE$), available potential energy ($APE$) and enstrophy ($EN$), and their spectral fluxes as a function of the two-dimensional wavenumber $n$ were computed for July 1979. Triangular truncation at zonal wavenumber 42 was used for computation. The slopes of various spectra in the wavenumber range $14 \leqslant n \leqslant 25$ were obtained by fitting a straight line in log–log scale by the least square method. The transient $KE$, $APE$ and $EN$ spectra in the lower (upper) troposphere had slopes $-2{\cdot}21$ ($-2{\cdot}30$), $-2{\cdot}65$ ($-2{\cdot}64$) and $-0{\cdot}36$ ($-0{\cdot}46$), respectively. The effect of stationary and divergent motion on the slope values was investigated. The possible correlation between the slope and percentage of transient component in the combined energy and enstrophy was examined to identify the transient motion of the atmosphere with the two-dimensional homogeneous isotropic turbulence. The vertically averaged slope of kinetic energy and enstrophy in the lower (upper) troposphere was close to the value at 700 (200) hPa level.

The spectral fluxes of kinetic energy and enstrophy in the wavenumber range $14 \leqslant n \leqslant 25$ satisfied, to a very rough approximation, the criteria of inertial subrange. The stationary fluxes were small. The estimated stationary-transient component of flux was larger, comparable and less than the corresponding transient flux of APE, KE and EN.

Representative levels for computation of energy and enstrophy spectra and their fluxes in the lower and upper troposphere were identified.

**Keywords.** Energy and enstrophy spectra; spectral fluxes; turbulent power laws; inertial subrange.

## 1. Introduction

To understand the dynamics of atmospheric motion, the observed energy and enstrophy spectra, nonlinear energy transfer between waves of different scales, conversion and dissipation terms are studied. The large scale atmospheric motions are quasi-horizontal. This is because the vertical velocity is at least three orders of magnitude less than the horizontal velocity. Much discussion about large scale atmospheric motion has been in terms of an idealised horizontal two-dimensional field. The horizontal motion contains a large range of spatial and temporal scales. For these reasons atmospheric motion is treated as a form of two-dimensional homogeneous turbulence. Homogeneous turbulence theory is applicable for free and mixing flows. The time mean of atmospheric flow does not vanish but has a large value. Hence we expect that the transient synoptic, subsynoptic scale motions can only be treated by the theory of two-dimensional homogeneous turbulence.

Theories of isotropic turbulence on a plane predict a $-3$ power law for kinetic and available potential energy spectra in the inertial subrange (Kraichnan 1967; Leith 1968; Charney 1971). If the kinetic energy spectrum follows a power law of the two-

dimensional index then one dimensional spectra will follow the same power law (Leith 1971). Baer (1972) introduced a two-dimensional index for spectral representation of global and hemispheric energy and demonstrated its appropriateness. The two-dimensional wavenumber index represents the degree of spherical harmonics and is obtained by summing over the order of the spherical harmonics for the same degree. Merilees (1979) showed that similar results hold for isotropic turbulence on a sphere. He has also shown that if the kinetic energy followed a $-3$ power law in terms of the two-dimensional wavenumber ($n$), then it follows the same power law for the zonal wavenumber ($m$) and meridional wavenumber ($n-m$). The enstrophy spectrum will follow a $-1$ power law.

Chen and Wiin–Nielsen (1978) computed the energy and enstrophy spectra and the associated spectral flux as a function of two-dimensional wavenumber for combined (stationary and transient) motion using data from the northern hemisphere for a winter. They found that the vertical mean slope of rotational kinetic energy spectrum was $-2{\cdot}6$. Boer and Shepherd (1983) presented explicitly rotational kinetic energy, available potential energy and enstrophy spectra for transient and stationary components of winter (January, 1979). The spectral slopes of kinetic and available potential energy obtained by Boer and Shepherd (1983) were less at all levels than those of Chen and Wiin–Nielsen (1978). The vertical profiles of slopes showed different characteristics. The difference in the results was ascribed to the differences in the data.

We wish to study the transient and stationary global spectra of energy and enstrophy, and the spectral fluxes during summer. We will try to bring out the salient differences between the lower and upper tropospheric features of the spectra. It will be relevant to identify the vertical levels where the spectral slope was closest to the theoretical values. The representative levels for the upper and lower troposphere were identified by the energy and enstrophy distribution.

## 2. Energy and enstrophy equations

The vorticity and thermodynamic equations of nondivergent, adiabatic, frictionless atmospheric motion in a rotating spherical coordinate system can be written as

$$\zeta_t + [a(1-\mu^2)]^{-1}(U\zeta)_\lambda + a^{-1}(V\zeta)_\mu + 2\Omega V/a = 0, \tag{1a}$$

$$T_t + [a(1-\mu^2)]^{-1}(UT)_\lambda + a^{-1}(VT)_\mu = 0, \tag{1b}$$

where $U = u\cos\varphi$, $V = v\cos\varphi$, $\mu = \sin\varphi$ and $\zeta = \nabla^2\Psi$. $\lambda$ represents the longitude and $\varphi$ is the latitude; $u$ and $v$ stand for the rotational part of zonal and meridional winds respectively, while $T$, $\zeta$ and $\Psi$ denote the temperature, relative vorticity and streamfunction. The subscripts are the variables with respect to which partial derivatives are taken. The second and third terms of the above equations are nonlinear interactions due to advection of vorticity and temperature. The earth is treated as a sphere of radius $a$.

The global rotational kinetic energy ($K$), enstrophy ($EN$) and available potential energy ($A$) per unit mass may be defined in terms of the streamfunction ($\Psi$) and temperature ($T$) by

$$K = (4\pi)^{-1}\int_{-1}^{1}\int_{0}^{2\pi}(-\Psi\nabla^2\Psi/2)\,\mathrm{d}\lambda\,\mathrm{d}\mu, \tag{2a}$$

$$EN = (4\pi)^{-1} \int_{-1}^{1} \int_{0}^{2\pi} (\zeta^2/2) \mathrm{d}\lambda \mathrm{d}\mu, \tag{2b}$$

$$A = (4\pi)^{-1} \int_{-1}^{1} \int_{0}^{2\pi} [gT^{*2}/(2\sigma)] \mathrm{d}\lambda \mathrm{d}\mu, \tag{2c}$$

where $T^*$ is the departure of temperature from its global mean, $\sigma$ is the static stability parameter given by

$$\sigma = g[\bar{T} C_p^{-1} - pR^{-1}(\partial \bar{T}/\partial p)], \tag{3}$$

where a bar stands for the area average and the other symbols have their usual meanings.

The real form of the spectral representation of $\Psi$ and $T^*$ for a fixed value of $p$ and $t$ using triangular truncation is expressed by

$$\Psi(\lambda, \mu) = \sum_{n=0}^{M} \sum_{m=0}^{n} (\Psi C_n^m \cos m\lambda + \Psi S_n^m \sin m\lambda) P_n^m(\mu), \tag{4a}$$

$$T^*(\lambda, \mu) = \sum_{n=0}^{M} \sum_{m=0}^{n} (TC_n^m \cos m\lambda + TS_n^m \sin m\lambda) P_n^m(\mu), \tag{4b}$$

where $\Psi C_n^m$, $TC_n^m$ are the cosine and $\Psi S_n^m$, $TS_n^m$ are the sine components of the spherical harmonic coefficients of streamfunction and temperature. These components are defined subsequently in section 3. Here $TC_0^0 = 0$, $P_n^m(\mu)$ is the associated Legendre function of first kind of order $m$ and degree $n$, normalised to unity over a unit sphere; $m$ is the zonal and $n$ the two-dimensional wavenumber, and $M$ is the truncation value for $m$ and $n$. Moreover,

$$\begin{aligned} \zeta C_n^m &= -n(n+1) a^{-2} \Psi C_n^m, \\ \zeta S_n^m &= -n(n+1) a^{-2} \Psi S_n^m, \end{aligned} \tag{5}$$

where $\zeta C_n^m$ and $\zeta S_n^m$ are cosine and sine components of spectral coefficients of $\zeta$.

### 2.1 *Energy and enstrophy spectra*

Substituting the spectral representations of $\Psi$ and $T^*$ in (2) and using (5), we get the following expressions for energy and enstrophy

$$K = \sum_{n=0}^{M} \sum_{m=0}^{n} K_n^m = \sum_{n=0}^{M} \sum_{m=0}^{n} n(n+1)(2 - \delta_{m0})(\Psi C_n^{m^2} + \Psi S_n^{m^2})(8a^2)^{-1}, \tag{6a}$$

$$EN = \sum_{n=0}^{M} \sum_{m=0}^{n} EN_n^m = \sum_{n=0}^{M} \sum_{m=0}^{n} n^2(n+1)^2(2 - \delta_{m0})(\Psi C_n^{m^2} + \Psi S_n^{m^2})(8a^4)^{-1}, \tag{6b}$$

$$A = \sum_{n=0}^{M} \sum_{m=0}^{n} A_n^m = \sum_{n=0}^{M} \sum_{m=0}^{n} (8\sigma)^{-1} g(2 - \delta_{m0})(TC_n^{m^2} + TS_n^{m^2}), \tag{6c}$$

where $\delta_{m0} = 0$ if $m = 0$ and $\delta_{m0} = 1$ if $m \neq 0$ and $A_0^0 = 0$. $K_n^m$, $EN_n^m$ and $A_n^m$ denote $K$, $EN$ and $A$ of the $(m, n)$ mode of motion.

The stationary and transient components of these spectra are defined by time averaging. The July mean of the spectral coefficients is the stationary part of the flow. It is necessary to note that the low frequency modes with a period of more than one month will have their contributions in the stationary as well as the transient spectra. Thus, the stationary (St) and transient (Tr) components of kinetic energy of the $(m, n)$ mode are

$$(K_n^m)_{\mathrm{St}} = n(n+1)[(\overline{\Psi C_n^m})^2 + (\overline{\Psi S_n^m})^2](8a^2)^{-1},$$
$$(K_n^m)_{\mathrm{Tr}} = n(n+1)\{[(\overline{\Psi C_n^m})']^2 + [(\overline{\Psi S_n^m})']^2\}(8a^2)^{-1}, \tag{6d}$$

where an overbar represents the time mean and a prime is the departure from the time mean.

By summing up over the longitudinal wavenumber $m$, $K$, $EN$ and $A$ can be expressed in terms of the two-dimensional wavenumber $n$. Thus, $K$, $EN$ and $A$ of the $n$th two-dimensional mode of motion are

$$K_n = \sum_{m=0}^{n} K_n^m, \tag{7a}$$

$$EN_n = \sum_{m=0}^{n} EN_n^m, \tag{7b}$$

$$A_n = \sum_{m=0}^{n} A_n^m. \tag{7c}$$

Similarly, by summing up over the two-dimensional wavenumber $n$, the $K$, $EN$ and $A$ of the $m$th zonal mode of motion are

$$K_m = \sum_{n=m}^{M} K_n^m, \tag{8a}$$

$$EN_m = \sum_{n=m}^{M} EN_n^m, \tag{8b}$$

$$A_m = \sum_{n=m}^{M} A_n^m. \tag{8c}$$

The vertically integrated zonal and two-dimensional spectra of energy or enstrophy in an atmospheric layer ($R$) between two pressure levels $p_L$ and $p_T$ are

$$(E_m)_R = g^{-1} \int_{p_T}^{p_L} E_m \mathrm{d}p,$$
$$(E_n)_R = g^{-1} \int_{p_T}^{p_L} E_n \mathrm{d}p, \tag{9}$$

where $p_L$ and $p_T$ indicate the pressures at the bottom and top of the atmospheric layer $R$.

### 2.2 *Wave–wave interactions*

The expression for the wave–wave interaction of $K$ is obtained from the kinetic energy equation in wavenumber domain. Hence, $K_n^m$ in (6a) is differentiated with

respect to time. Thus,

$$(K_n^m)_t = n(n+1)(2-\delta_{m0})[\Psi C_n^m(\Psi C_n^m)_t + \Psi S_n^m(\Psi S_n^m)_t](4a^2)^{-1}. \tag{10}$$

The spectral form of the vorticity equation, i.e. of (1a), is obtained by substituting the spectral representations of the variables involved. This in turn is used to obtain the tendencies of spectral coefficients of the streamfunction. Therefore, (10) becomes

$$(K_n^m)_t = NK_n^m, \tag{11a}$$

where

$$NK_n^m = (2-\delta_{m0})(\Psi C_n^m IC_n^m + \Psi S_n^m IS_n^m)/4. \tag{11b}$$

$NK_n^m$ represents the gain of kinetic energy by the $(m,n)$ mode of motion due to nonlinear interactions. This includes the wave-zonal flow as well as the wave–wave interactions. $IC_n^m$ and $IS_n^m$ are the spherical harmonic coefficients of the advection terms of the vorticity equation, where

$$I = [a(1-\mu^2)]^{-1}(U\zeta)_\lambda + a^{-1}(V\zeta)_\mu. \tag{12}$$

Summing of (11a) over the longitudinal wavenumber $m$ gives the kinetic energy equation in the two-dimensional wavenumber domain. Thus,

$$(K_n)_t = \sum_{m=0}^{n}(2-\delta_{m0})(\Psi C_n^m IC_n^m + \Psi S_n^m IS_n^m)/4. \tag{13a}$$

The enstrophy equation is obtained from $EN_n^m$ in (6b) by following the same procedure. On differentiating (6c) with respect to time and using the spectral form of thermodynamic equation to compute the tendencies of spectral coefficients of $T^*$, the available potential energy equation is obtained. Thus, the enstrophy and available potential energy equations in the two-dimensional spectral domain are

$$(EN_n)_t = -\sum_{m=0}^{n}(2-\delta_{m0})(\zeta C_n^m IC_n^m + \zeta S_n^m IS_n^m)/4, \tag{13b}$$

$$(A_n)_t = -g(4\sigma)^{-1}\sum_{m=0}^{n}(2-\delta_{m0})(TC_n^m JC_n^m + TS_n^m JS_n^m), \tag{13c}$$

where $JC_n^m$ and $JS_n^m$ are the spectral coefficients of the advection terms ($J$) of the thermodynamic equation (1b). Here,

$$J = [a(1-\mu^2)]^{-1}(UT)_\lambda + a^{-1}(VT)_\mu. \tag{13d}$$

### 2.3 *Spectral fluxes*

In the absence of dissipation and forcings, the rotational kinetic energy ($K$) and enstrophy ($EN$) are conservative quantities. This implies that

$$\sum_{n=0}^{M}\sum_{m=0}^{n} NK_n^m = \sum_{n=0}^{M} NK_n = 0, \tag{14a}$$

$$\sum_{n=0}^{M}\sum_{m=0}^{n} n(n+1)a^{-2}NK_n^m = \sum_{n=0}^{M} n(n+1)a^{-2}NK_n = 0, \tag{14b}$$

where

$$NK_n = \sum_{m=0}^{n} NK_n^m. \tag{14c}$$

From (14a) and (14b) we see that the nonlinear interactions only redistribute energy and enstrophy among the wavenumbers without any net change. We can divide $NK_n$ in two intervals of wavenumber, namely $(0, v)$ and $(v+1, M)$. We write (14a) as

$$\sum_{n=0}^{v} NK_n + \sum_{n=v+1}^{M} NK_n = 0,$$

or

$$\sum_{n=0}^{v} NK_n = -\sum_{n=v+1}^{M} NK_n. \tag{15}$$

Thus the energy loss by the wavenumber group $(0, v)$ is equal to the gain by the wavenumber group $(v+1, M)$. Noting that a positive flux implies outward transfer of energy (towards larger $n$), the spectral flux of kinetic energy is defined by

$$KF(n) = -a^{-1} \sum_{v=0}^{n} NK_v. \tag{16a}$$

Similarly, the enstrophy and available potential energy fluxes are defined by

$$ENF(n) = -a^{-3} \sum_{v=0}^{n} v(v+1)NK_v, \tag{16b}$$

$$AF(n) = -a^{-1} \sum_{v=0}^{n} \left( \sum_{m=0}^{n} NA_v^m \right), \tag{16c}$$

where

$$NA_v^m = (2 - \delta_{m0})(TC_v^m JC_v^m + TS_v^m JS_v^m)/4\sigma. \tag{17}$$

## 3. Data and analysis

### 3.1 *Observational data*

The data consist of the daily uninitialized FGGE III-b level global analyses of geopotential height, and zonal and meridional components of wind for July 1979. The data were available at 1·875° latitude-longitude grid on 15 standard pressure levels (i.e. 1000, 850, 700, 500, 400, 300, 250, 200, 150, 100, 70, 50, 30, 20 and 10 hPa) for 4 synoptic hours. The analyses on 10 pressure levels from 1000 to 100 hPa at 12 GMT were used in this study.

### 3.2 *Analysis procedure*

The spectral coefficients of streamfunction, velocity potential and of the departure of temperature from its area average were calculated to obtain the global average energy and enstrophy spectra. For this purpose, the daily global analyses of wind components and geopotential height were used. The following set of equations was used to transform

the variables between physical and spectral domains.

$$Z(\lambda,\mu)=\sum_{n=0}^{M}\sum_{m=0}^{n}(ZC_n^m\cos m\lambda+ZS_n^m\sin m\lambda)P_n^m(\mu),$$

where

$$ZC_n^m=\pi^{-1}\int_{-1}^{1}\int_{0}^{2\pi}Z(\lambda,\mu)\cos m\lambda P_n^m(\mu)\mathrm{d}\lambda\,\mathrm{d}\mu,$$

$$ZS_n^m=\pi^{-1}\int_{-1}^{1}\int_{0}^{2\pi}Z(\lambda,\mu)\sin m\lambda P_n^m(\mu)\mathrm{d}\lambda\,\mathrm{d}\mu,\quad \text{for } m>0,$$

$$ZC_n^0=(2\pi)^{-1}\int_{-1}^{1}\int_{0}^{2\pi}Z(\lambda,\mu)P_n^0(\mu)\mathrm{d}\lambda\,\mathrm{d}\mu,\quad ZS_n^0=0. \tag{18}$$

The procedure involves an efficient Fourier transform along Gaussian latitudes and a Legendre transform along the meridional direction using Gaussian quadrature. For triangular truncation at $M$, $(M+1)$ Gaussian latitudes were needed for meridional integration. Gaussian latitudes, which are the zeros of Legendre polynomials of order $M+1$, were obtained by Newton-Raphson's iterative method. In transforming the grid point analyses onto Gaussian latitudes, cubic splines were used. Further, a triangular truncation at $M=42$ was used to obtain spectral coefficients.

### 3.3 *Spherical harmonic analysis*

3.3a *Horizontal wind field*: As suggested by Robert (1966), the horizontal components of the vector wind $V$ were replaced by suitable scalar variables

$$U=-a^{-1}(1-\mu^2)\Psi_\mu+a^{-1}\chi_\lambda,$$
$$V=a^{-1}\Psi_\lambda+a^{-1}(1-\mu^2)\chi_\mu. \tag{19a}$$

It is important to note here that in computing the energy and enstrophy, the spectral coefficients of vorticity and divergence were obtained from the total (rotational + divergent) $u$ and $v$ fields. In the computations of the nonlinear interactions and fluxes, however, only the rotational part of the wind components was used. The symbols $U$ and $V$ to represent $u\cos\varphi$ and $v\cos\varphi$ remained unchanged in both the cases.

We then have

$$\zeta=[a(1-\mu^2)]^{-1}V_\lambda-a^{-1}U_\mu. \tag{19b}$$

On substituting spectral expansions for $U$ and $V$ in (19a), and on the application of (i) the standard recurrence relation for $\mathrm{d}P_n^m/\mathrm{d}\mu$ and (ii) the orthogonality of the harmonics, we get the relationships

$$\zeta C_n^m=[a(1-\mu^2)]^{-1}[mVS_n^m-n\varepsilon_{n+1}^m UC_{n+1}^m+(n+1)\varepsilon_n^m UC_{n-1}^m],$$
$$\zeta S_n^m=[a(1-\mu^2)]^{-1}[-mVC_n^m-n\varepsilon_{n+1}^m US_{n+1}^m+(n+1)\varepsilon_n^m US_{n-1}^m], \tag{20}$$

where

$$\varepsilon_n^m=[(n^2-m^2)/(4n^2-1)]^{1/2}.$$

Spectral coefficients of vorticity were computed using (20), from the spectral coefficients of $U$ and $V$. Finally, the spectral coefficients of streamfunction were obtained from those of vorticity using (5).

For studying the global spectra of the divergent part of kinetic energy, the spectral coefficients of velocity potential ($\chi$) were obtained from those of divergence ($D$) following the same procedure used for the streamfunction. The spectral relationships are

$$DC_n^m = [a(1-\mu^2)]^{-1}[mUS_n^m + n\varepsilon_{n+1}^m VC_{n+1}^m - (n+1)\varepsilon_n^m VC_{n-1}^m],$$
$$DS_n^m = [a(1-\mu^2)]^{-1}[-mUC_n^m + n\varepsilon_{n+1}^m VS_n^m - (n+1)\varepsilon_n^m VS_{n-1}^m], \quad (21)$$

where

$$D = \nabla^2\chi = [a(1-\mu^2)]^{-1}U_\lambda + a^{-1}V_\mu. \quad (22)$$

3.3b *Geopotential height*: The spectral coefficients of geopotential height were obtained by using (18). The hydrostatic approximation was used to obtain the spectral coefficients of temperature. Thus,

$$TC_n^m = -(g/R)\left[\frac{\partial}{\partial(\log p)}(ZC_n^m)\right],$$
$$TS_n^m = -(g/R)\left[\frac{\partial}{\partial(\log p)}(ZS_n^m)\right]. \quad (23)$$

The derivative with respect to $\log p$ at standard pressure levels was obtained by using cubic splines.

### 3.4 *Static stability parameter*

The earlier diagnostic studies on available potential energy e.g. Baer (1972), Chen and Wiin-Nielsen (1978) have used values of the static stability parameter given by Gates (1961). In this study, the static stability parameter was computed from the present data. The relevant expression for this is given by equation (3). The time mean of the global average temperature for July 79 was used to represent $\bar{T}$ in equation (3). The vertical gradient of $\bar{T}$ with respect to $\log p$ at all standard pressure levels was obtained by cubic splines.

### 3.5 *Evaluation of spectral slope and vertical integration*

A forced two-dimensional turbulence in which kinetic energy is injected at a certain rate at a fixed wavenumber ($n_s$) contains two inertial subranges. In the first ($n < n_s$) the kinetic energy follows a $-5/3$ power law and in the second ($n > n_s$) it follows a $-3$ power law (Lesieur 1987). We have considered provisionally the wavenumber range $14 \leqslant n \leqslant 25$ as the inertial subrange where baroclinically forced eddies do not exist. The energy follows $-3$ power law and enstrophy follows $-1$ power law in this range. This range was also used as inertial subrange by earlier workers. The power law followed by the energy and enstrophy spectra in the inertial subrange is of the form

$$E_k = ak^b, \quad (24)$$

where $E_k$ stands for the energy or enstrophy of the $k$th component of spectra, $k$ is the zonal or two-dimensional wavenumber, and $a$ and $b$ are constants. To find the slope $b$, the computed observed energy and enstrophy spectra in a given domain were fitted with a straight line for the variables log $E_k$ and log $k$ by least squares.

The vertical integral in (9) was expressed as the sum of integrals between consecutive standard pressure levels. The integration between consecutive levels was performed numerically by the trapezoidal rule.

### 3.6 *Spectral representation of nonlinear terms*

The spectral coefficients of nonlinear terms of the vorticity and thermodynamic equations were obtained numerically by using the half transform method (Eliasen *et al* 1970). In this method, the Fourier representation (transform) of a nonlinear product term along the Gaussian latitude was obtained as a product of their Fourier series. The Fourier series, in turn, were obtained by the Legendre inverse transform. The Legendre transform along a meridian was numerically obtained by Gaussian quadrature. For triangular truncation at $M$, the Fourier coefficients of variables at $(3M + 1)/2$ Gaussian latitudes were computed.

## 4. Results

In the following discussion the atmospheric layers (1000–500) hPa and (500–150) hPa were identified as the lower troposphere and the upper troposphere. The energy and enstrophy were computed per unit mass in units of joules/kg, while the nonlinear interactions, and the spectral energy and enstrophy fluxes were presented as vertically integrated quantities for a unit horizontal area on the spherical earth.

### 4.1 *Energy and enstrophy*

The rotational stationary and transient kinetic energy spectra for the lower and upper tropospheres are presented on a log–log scale in figures 1(a) and (b). The transient kinetic energy has a broad peak in the interval $6 \leqslant n \leqslant 10$. Further, the transient component of the flow dominates for $n > 10$, while for $n \leqslant 5$ the stationary component dominates the flow. The two components are comparable for $5 \leqslant n \leqslant 10$. The stationary and transient components of available potential energy spectra for the lower and upper troposphere are presented in figures 2(a) and (b). The stationary component dominates over the transient component for $n < 4$ in the lower as well as the upper troposphere. This is similar to the kinetic energy spectra. The transient component is dominant for $n > 10$ by a comparatively small magnitude, which is even less than that for the transient kinetic energy spectra. The stationary and transient components are comparable for $5 \leqslant n \leqslant 9$.

Thus, the scale separation between the transient and stationary flows of the atmosphere during the northern summer was noticed. In the northern winter, the scale separation was much sharper (Boer and Shepherd 1983). Lambert (1984) has shown that a broad maximum near wavenumber 10 also occurs in the APE-KE conversion due to energy conversion in synoptic scale disturbances. This justified the choice of the inertial subrange between $14 \leqslant n \leqslant 25$.

The slope of rotational kinetic energy as a function of pressure for transient,

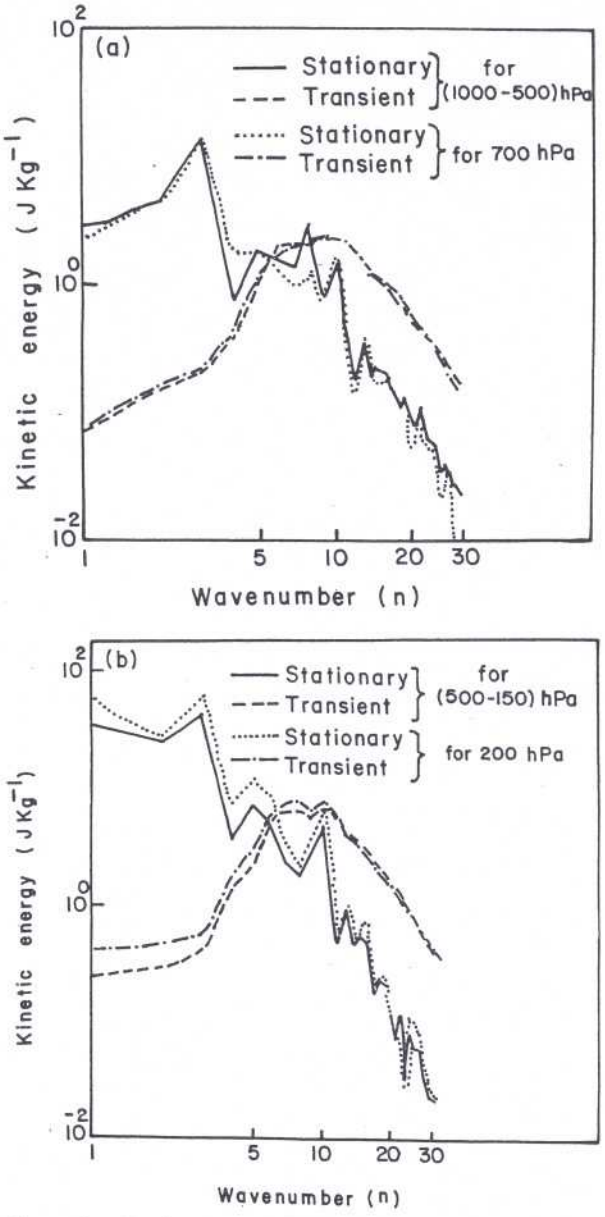


**Figure 1.** Stationary and transient components of global average rotational kinetic energy spectra over the (**a**) lower troposphere (**b**) upper troposphere during July 1979.

stationary and combined motion is shown in figure 3. We find that the slope of transient kinetic energy spectrum was closest to the $-3$ power law at 150 hPa. The lower and upper tropospheric spectra of rotational transient kinetic energy in the range $14 \leqslant n \leqslant 25$ exhibit vertical mean slopes of $-2{\cdot}21$ and $-2{\cdot}30$ respectively. We note that the transient divergent kinetic energy spectra have slopes $-1{\cdot}41$ and $-1{\cdot}65$ in the lower and upper troposphere. These slopes are less than the corresponding values for the rotational spectra. To compare the slopes with those of Chen and Wiin-Nielsen (1978), we also computed the slope of rotational kinetic energy spectrum for the combined motion. The slope was $-2{\cdot}22$ ($-2{\cdot}47$) in the lower (upper) troposphere.

To identify the main features of the kinetic energy spectra which were responsible

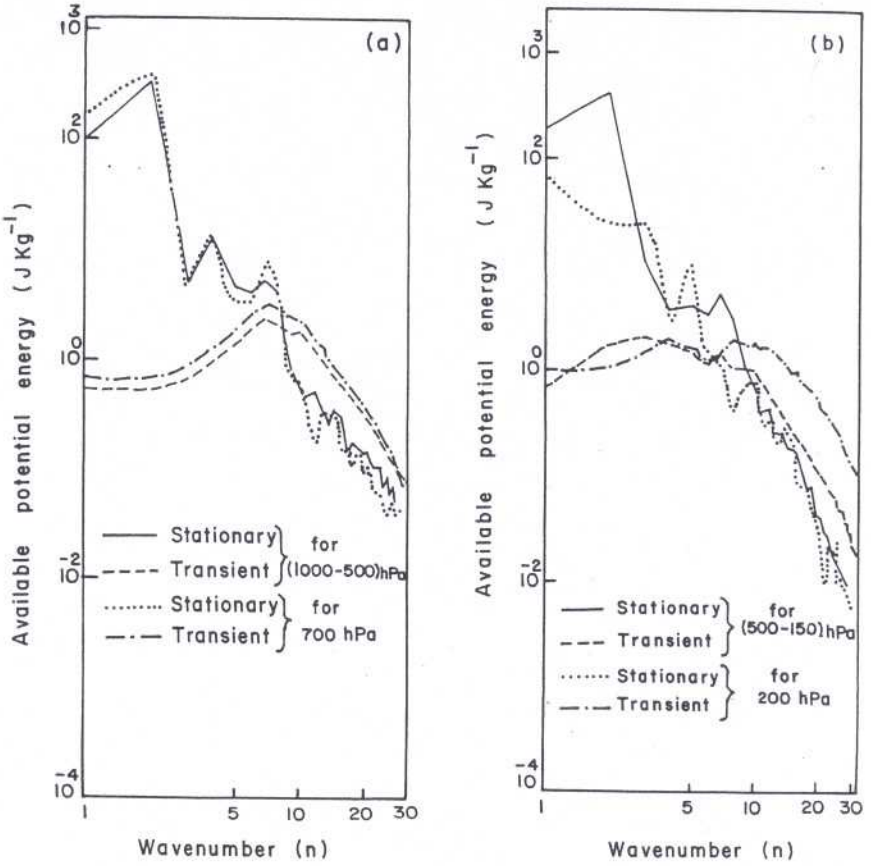


**Figure 2.** (a) and (b) are same as figures 1(a) and (b) for available potential energy.

for a larger slope in the upper troposphere than in the lower troposphere the two spectra were closely examined. We found that compared to the lower troposphere, the increase of kinetic energy for wavenumbers at the lower end of inertial subrange was more than the increase of kinetic energy for wavenumbers at the upper end in the upper troposphere. If the largest value in the inertial subrange was normalised to the same value, the lower value of slope in the lower troposphere compared to the value in the upper troposphere indicates that the smaller scale eddies have more kinetic energy in the former than in the latter. Even though the difference between lower tropospheric and upper tropospheric slopes was numerically small, considering the theoretical value of $-3$ for the slope, it is more prominent for the combined motion than for transient motion (table 1). The slopes in the lower and upper troposphere as well as the difference between them were less compared to the values obtained by Chen and Wiin-Nielsen (1978).

The stationary rotational kinetic energy spectrum in the lower (upper) troposphere displayed a $-2{\cdot}32$ ($-4.19$) power law. For the stationary divergent spectra the slope values were $-1{\cdot}43$ and $-2{\cdot}26$ in the lower and upper troposphere. Thus, both the stationary rotational and divergent components showed a large difference in their lower and upper tropospheric slopes in comparison with their theoretical value. The kinetic energy spectra of the total (rotational + divergent) wind of combined motion has slopes of $-2{\cdot}18$ and $-2{\cdot}45$ for the lower and upper troposphere. Table 1 shows that the slope values for the rotational kinetic energy and for the (rotational +

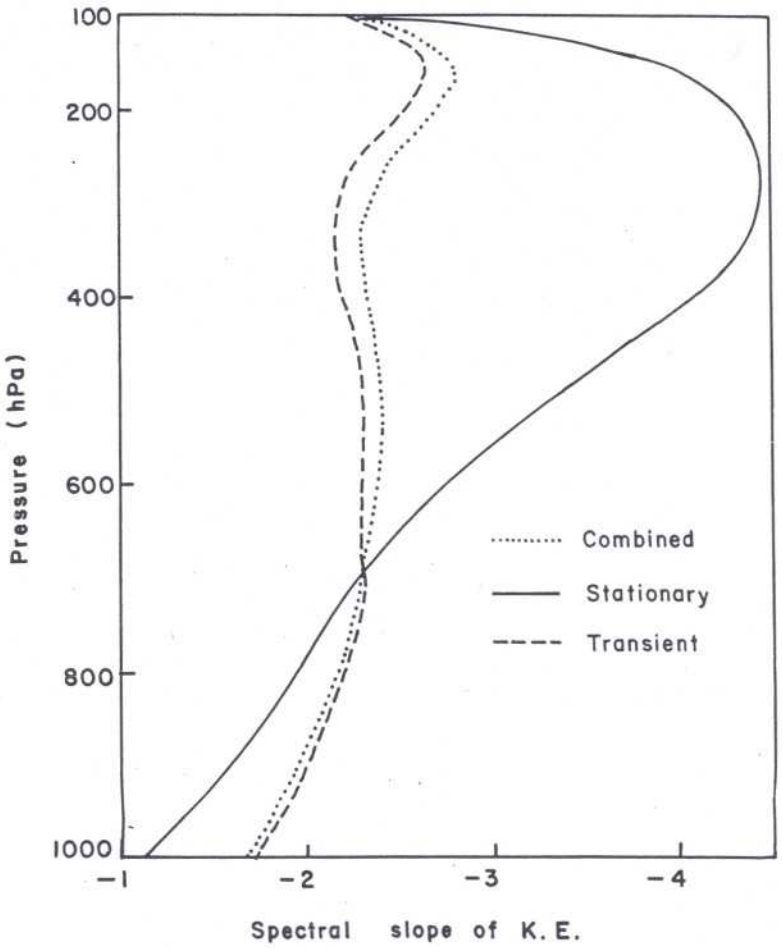


**Figure 3.** Vertical distribution of slope of rotational kinetic energy.

**Table 1.** Slope of energy and enstrophy in the wavenumber domain $14 \leqslant n \leqslant 25$.

| | Rotational KE | | Divergent KE | | (Rotational + Divergent) KE | | APE | | Enstrophy | |
|---|---|---|---|---|---|---|---|---|---|---|
| | LT | UT | LT | UT | LT | UT | LT | UT | LT | UT |
| Combined motion | −2·22 | −2·47 | −1·72 | −1·71 | −2·18 | −2·45 | −2·53 | −2·83 | −0·37 | −0·63 |
| Stationary | −2·32 | −4·19 | −1·43 | −2·26 | −2·20 | −4·08 | −2·24 | −4·34 | −0·45 | −2·27 |
| Transients | −2·21 | −2·30 | −1·41 | −1·65 | −2·17 | −2·29 | −2·65 | −2·62 | −0·36 | −0·46 |

LT: Lower troposphere.
UT: Upper troposphere.

divergent) kinetic energy were quite close. This shows that the slope values do not change significantly by inclusion of the divergent part of kinetic energy. In other words, the influence of divergent motion on the slopes of kinetic energy in the inertial subrange is insignificant. This may be attributed to the fact that the divergent kinetic energy was more than an order of magnitude less than the rotational kinetic energy (table 2). The slope of the combined spectra was slightly more by less than 10% of the value for transient spectra in the upper troposphere. But the slope for the stationary

**Table 2.** Global averaged kinetic energy (Unit: J/Kg).

| | Stationary | | | | Transient | | | |
|---|---|---|---|---|---|---|---|---|
| | Rotational | | Divergent | | Rotational | | Divergent | |
| | (KZ) | (KE) | (KZ) | (KE) | (KZ) | (KE) | (KZ) | (KE) |
| Lower troposphere | 23·59 | 9·45 | 0·32 | 0·87 | 1·52 | 27·54 | 0·05 | 1·16 |
| Upper troposphere | 121·60 | 19·16 | 0·28 | 0·78 | 3·65 | 76·30 | 0·09 | 2·47 |

KZ: Zonal kinetic energy.
KE: Eddy kinetic energy.

spectra was nearly twice the value for transient spectra. This is because of the relatively small kinetic energy of stationary motion compared to the transient motion in wavenumber range $14 \leqslant n \leqslant 25$. Baer (1972) obtained a value of $-3$ for the vertical mean slope in the layer 700–200 hPa for kinetic energy of the total wind and combined motion, but in our case the value was $-2{\cdot}42$. The average slope in the lower troposphere was close to the value for 700 hPa, while the value at 250 hPa was close to the average value for the upper troposphere.

The departure of the transient kinetic energy spectra in the inertial subrange from the $-3$ law may be due to the non-inclusion of unresolved small zonal scales from the data and the distortion in the small scales due to the observations and the analysis. To arrive at the above conclusion we need to know the effect of truncation on computation of energy and enstrophy spectra. For this purpose, the spectra may be computed with different truncation values. This aspect will be explored in a subsequent study.

The spectrum of transient available potential energy has a slope of $-2{\cdot}65$ ($-2{\cdot}62$) in the lower (upper) troposphere. The available potential energy spectra were closer to $-3$ power law compared to kinetic energy. The slopes of transient available potential energy spectrum were very close to $-3$ in the 600–400 hPa layer (figure 4). The maximum departure from $-3$ power law for transient cases was observed at 250 hPa. The vertical variation of the slope shows two maxima at 100 hPa and 500 hPa with the upper maximum having a larger value ($-3{\cdot}37$) than the lower maximum value ($-2{\cdot}80$). Minima with decreasing magnitudes were located at 1000 hPa and 250 hPa.

The slopes for the stationary spectrum of available potential energy in the lower and upper troposphere were $-2{\cdot}24$ and $-4{\cdot}34$ respectively. The large difference in the two values was due to a sharp decrease in the APE at the upper end of the inertial subrange in the upper troposphere than the lower troposphere with approximately the same APE at the lower end. The spectra for combined motion have slopes of $-2{\cdot}53$ and $-2{\cdot}83$ in the lower and upper troposphere. The slope of combined available potential energy exhibits two maxima of $-3{\cdot}53$ and $-2{\cdot}99$ at 100 hPa and 400 hPa respectively. APE slope for July 1979 was much larger than that of January 1979 obtained by Boer and Shepherd (1983). Further, it may be added that the average slope of APE in the lower troposphere was in good agreement with a value somewhere between 850 and 700 hPa. The upper tropospheric value was in agreement with the value somewhere between 200 and 150 hPa.

The slopes of transient enstrophy spectra for the lower and upper tropospheres were $-0{\cdot}36$ and $-0{\cdot}46$. These values were considerably less than the theoretical value of $-1$. They were even less than the hemispheric value of $-0{\cdot}6$ obtained by

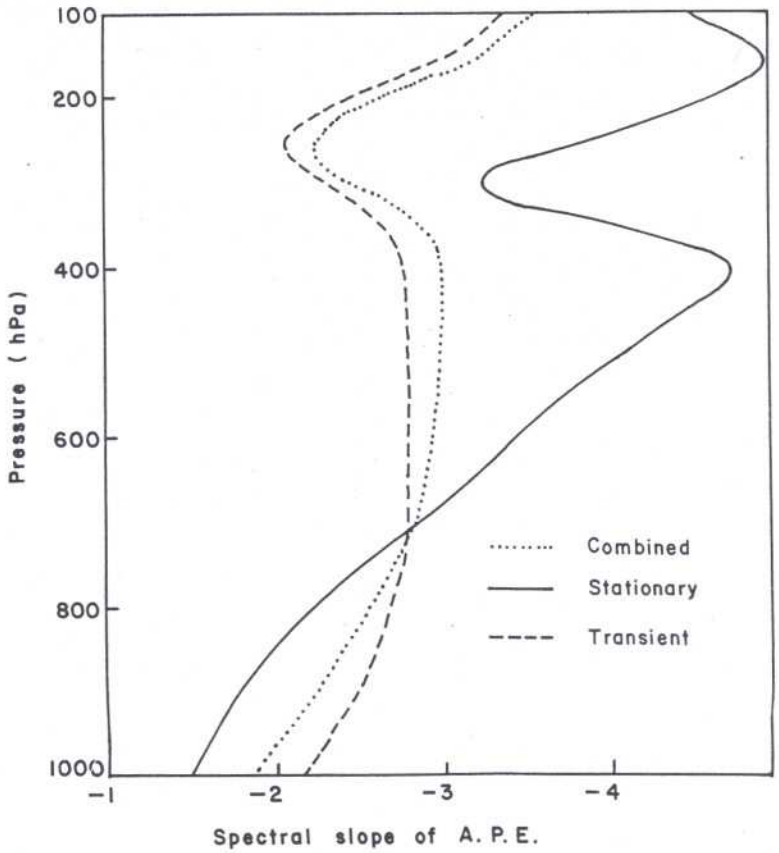


**Figure 4.** Same as figure 3 for available potential energy.

Chen and Wiin-Nielsen (1978). The largest negative value of slope for transient enstrophy was $-\cdot 80$ and located at 150 hPa (figure 5). It may be stated with reference to the slope of the enstrophy spectra for combined motion that the slope values in the lower and upper troposphere were close to the 700 and 250 hPa values. We found (figures 3 through 5) from the comparison of the slopes of stationary and transient spectra that the slope of the stationary energy and enstrophy spectra was less while its departure from the theoretical values was more in the lower troposphere. In the upper troposphere the slope as well as its departure from the theoretical values for stationary spectra were more compared to that for transient spectra.

We computed the slope of $m$ spectra of kinetic energy, available potential energy and enstrophy in the zonal wavenumber range $8 \leqslant m \leqslant 16$ (not presented). In the choice of this range, we considered the length scale implied by the two-dimensional wavenumber range chosen in this study. Taking zonal scale along 45° latitude as the mean, $m$ range corresponding to the $n$ range is fixed. A comparison between the slopes for $m$ and $n$ spectra reveals that the slopes of the $m$ spectra were closer to the theoretical values than the $n$ spectra.

To examine the correlation between the strength of transient motion and its closeness to the $-3$ law, the percentage of transient in the combined motion was computed for the rotational kinetic, available potential energy and enstrophy. They are presented as a function of $p$ in figure 6. For kinetic energy the contribution of the transients decreased monotonically with height from a value of 54·4% at 1000 hPa to a value of 17·5% at 100 hPa. The values for the lower and upper tropospheres

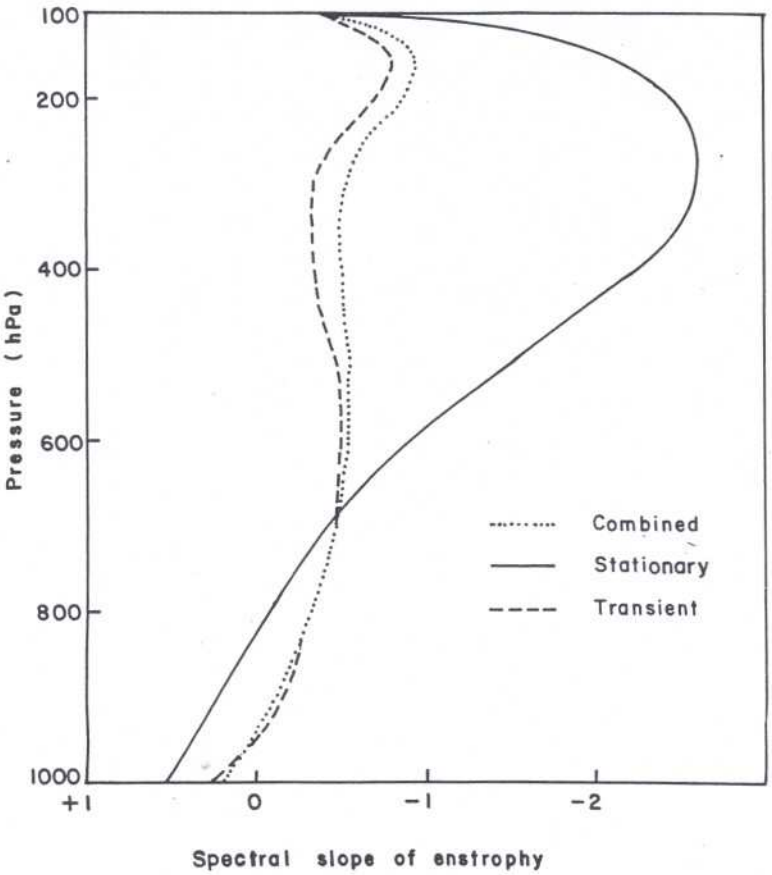


**Figure 5.** Same as figure 3 for enstrophy.

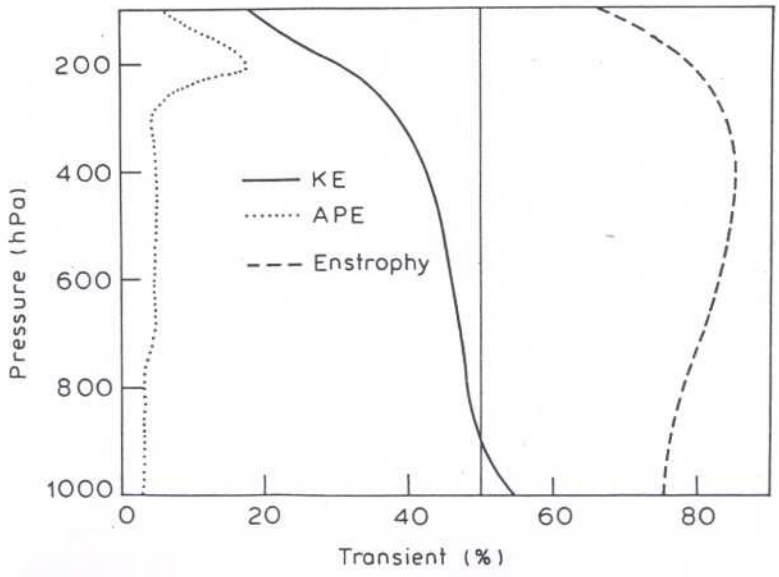


**Figure 6.** Percentage of transient energy and enstrophy in the combined motion shown as a function of pressure.

were 46·8% and 36·2%. For enstrophy, the maximum percentage value of 85% was located at 400 hPa. It decreased in both directions reaching a value of 75·3% at 1000 hPa and 59% at 100 hPa. The percentage contribution for transient available potential energy attained a maximum value of 17·7% at 200 hPa and monotonically decreased in both directions reaching a minimum value of 3·5% at 1000 hPa. The value at 100 hPa was 6·7%. The high contribution of transients in the combined enstrophy indicated that stationary motion was essentially a low wavenumber phenomenon while the transient motion was a relatively high wavenumber phenomenon. This confirmed the conclusion arrived from the kinetic energy spectra.

The slope of the total kinetic energy spectrum at each level was examined for a possible correlation between the percentage of transient kinetic energy and its closeness to the $-3$ law. It was noticed by comparing figures 3 and 6 that in the troposphere while the percentage of transient kinetic energy was maximum at 1000 hPa and minimum at 100 hPa, the deviation of slope from $-3$ law was maximum at 1000 hPa and minimum at 150 hPa. The same conclusion was reached for APE and enstrophy. It seems that the slopes of transient energy and enstrophy spectra were closest to the theoretical values at 150 hPa.

The representative levels for the vertically averaged energy and enstrophy spectra in the lower and upper troposphere were identified by comparing these with the spectra at 700 and 200 hPa. We found that 700 hPa was a good representative level for the lower troposphere for both *KE* and *APE*. 200 hPa was a representative level for the upper troposphere for *KE* but not for *APE* (figures 1 and 2).

### 4.2 *Spectral fluxes*

In a two-dimensional isotropic homogeneous turbulence, only a fraction of the energy can flow to smaller scales and a greater fraction has to flow simultaneously to larger scales (Fjortoft 1953). Due to enstrophy conservation in a two-dimensional flow, the energy cascade to smaller scales is prevented by vortex stretching. This is in contrast with the three dimensional turbulent flow where there is a down-scale flow of kinetic energy due to vortex tube stretching. The inertial subrange postulated by Kraichnan (1967) for a two-dimensional turbulence is then characterised by a uniform transfer of energy to lower wavenumbers and enstrophy to higher wavenumbers. Thus, a constant positive flux of enstrophy and a vanishing flux of energy are associated with the energy spectrum which follows a $-3$ power law.

Pure transient and stationary components of the kinetic energy flux were computed by using the transient and stationary streamfunction. Table 3 shows fluxes of kinetic

**Table 3.** Spectral fluxes of energy and enstrophy in different two-dimensional wave categories.

| | | Kinetic energy ($10^{-3}$ W m$^{-2}$) | | | Enstrophy ($10^{-13}$ kg m$^{-2}$ s$^{-3}$) | | |
|---|---|---|---|---|---|---|---|
| | $n\rightarrow$ | 1–13 | 14–25 | 26–42 | 1–13 | 14–25 | 26–42 |
| Total | LT | −1·12 | −0·18 | 0·37 | −0·81 | 66·72 | 150·80 |
| | UT | −2·99 | −0·42 | 0·93 | 4·66 | 164·40 | 372·50 |
| Stationary | LT | −0·08 | 0·01 | 0·01 | 0·51 | 4·19 | 4·91 |
| | UT | −0·21 | 0·05 | 0·01 | 3·29 | 8·31 | 4·93 |
| Transient | LT | −0·42 | −0·19 | 0·23 | −5·28 | 29·75 | 92·00 |
| | UT | −1·03 | −0·53 | 0·60 | −13·60 | 71·25 | 242·80 |

energy and enstrophy in different wave categories. The total and transient flux of energy in the inertial subrange followed the criterion of zero flux more closely as compared to the other wave categories. The enstrophy flux is down the scale in the inertial subrange as expected from the theory of two-dimensional turbulence.

The transient, stationary and total flux of rotational kinetic energy for the lower and upper troposphere are presented in figures 7(a) and (b) respectively. The stationary

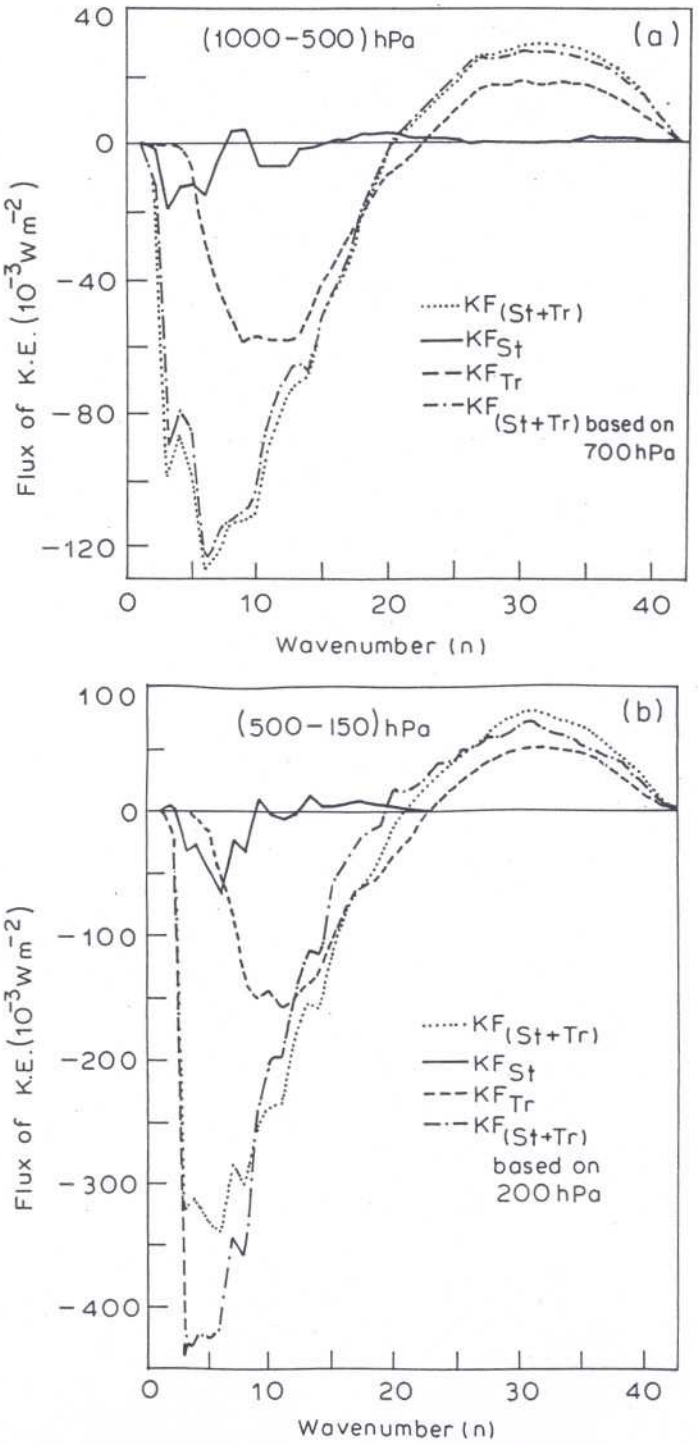


**Figure 7.** Vertically integrated stationary and transient components of spectral fluxes of global rotational kinetic energy over the **(a)** lower troposphere **(b)** upper troposphere during July 1979.

component of the flux was negligible compared to the transient and total flux. The largest negative stationary flux in the troposphere was significantly less than the value obtained by Shepherd (1987) for the winter (January, 1979). Further, up the scale stationary flux was essentially confined in the wavenumber interval $3 \leqslant n \leqslant 9$. Thus, the stationary nonlinear interaction was weak and confined to the large scale. It was approximately local in nature in the spectral space. The stationary component of kinetic energy flux was almost zero in the wavenumber interval $14 \leqslant n \leqslant 25$. The criterion for the existence of an inertial subrange for kinetic energy flux was satisfied by stationary motion, which was not a part of turbulence.

The transient and total flux of kinetic energy was up the scale for $n < 22$ and down the scale for $n > 22$. In the wavenumber range $14 \leqslant n \leqslant 25$, the flux was very weak compared to the largest positive and negative values. The kinetic energy flux in the upper troposphere was 2·5 times more than that in the lower troposphere, while the difference between slopes of transient kinetic energy spectrum in the lower and upper troposphere is insignificant. The ratio of the largest positive flux to the largest negative flux was approximately the same for the lower and upper troposphere. The ratio was 3:1 for transient component of kinetic energy flux and 4:1 for total flux. The largest negative value of the transient flux in the troposphere ($-210 \times 10^{-3}\,\mathrm{Wm}^{-2}$) was about 30% less than the value for January 1979 (Shepherd 1987). This was also true for the total flux in the troposphere.

Figures 7(a) and (b) suggest that the stationary, transient and total rotational kinetic energy fluxes vanish at the truncation wavenumber $n = 42$. This implies that the sum of nonlinear kinetic energy interaction over the entire resolved wavenumber range $0 \leqslant n \leqslant 42$ for stationary and transient motion vanishes. Thus, the stationary–stationary, transient–transient energy transfer processes behave in a true sense as nonlinear interactions, which only redistribute kinetic energy among the different resolved wavenumbers without generating any net kinetic energy. Shepherd (1987) has shown that the total energy and enstrophy flux can be expressed as the sum of stationary, transient and mixed stationary–transient fluxes. The mixed stationary–transient fluxes arise due to the interactions between the stationary and transient waves. It has been noted that the stationary flux of kinetic energy can be neglected in comparison with the transient and total fluxes. It can be concluded that the maximum up scale stationary–transient flux of kinetic energy was more than the maximum transient flux in both the lower and upper tropospheres.

To compare the kinetic energy flux at 700(200) hPa with the flux in the lower (upper) troposphere we have computed the flux in the layer by assuming the constant value of kinetic energy flux at 700(200) hPa throughout the layer. We note that 700 hPa was a good representative level of the lower troposphere for the kinetic energy flux. The largest negative kinetic energy flux based on 200 hPa was larger than the value for the upper troposphere. The up scale flux in the upper troposphere based on 200 hPa in a part of inertial subrange $9 \leqslant n \leqslant 19$ was less compared to the upper tropospheric value. Thus, the criterion of inertial subrange was better satisfied by the 200 hPa flux in comparison to the upper troposphere. It may be mentioned that the slope at 200 hPa was closer to $-3$ than that for the upper troposphere.

The $n$ spectra of enstrophy flux for the lower and upper troposphere are presented in figures 8(a) and (b). A strong down the scale flux of enstrophy was observed for $n > 15$ while a weak up the scale flux was confined to the low wavenumbers $n < 15$. It was an order of magnitude smaller than the maximum flux. The up scale transient

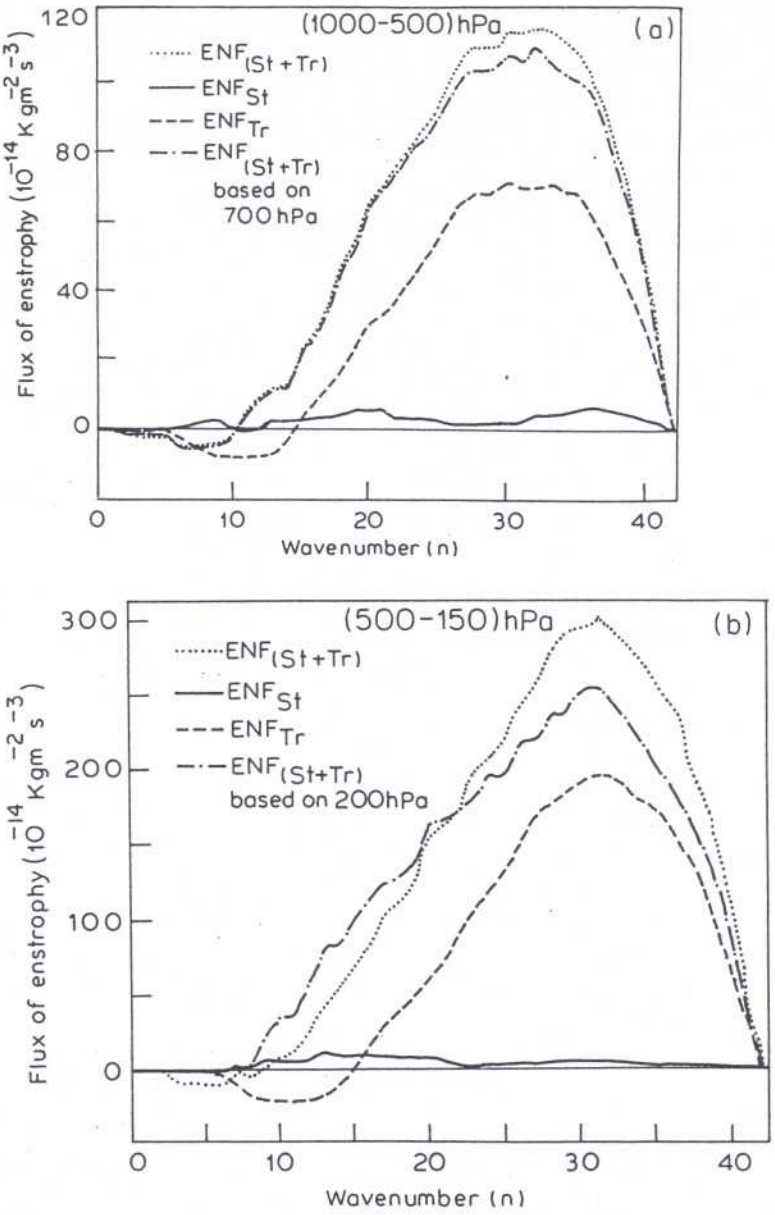


**Figure 8.** (**a**) and (**b**) are same as figures 7(a) and (b) for enstrophy.

fluxes in the low wavenumbers were comparatively stronger than the total fluxes. The transient enstrophy flux was moving away from wavenumber $n = 15$. The stationary flux of enstrophy was negligibly small compared to the transient and total fluxes. The fluxes were strong in the upper troposphere compared to those in the lower troposphere. The maximum transient and total fluxes in the upper troposphere were about 1 to 3 times the corresponding value in the lower troposphere. The fluxes which were more than 20% of the maximum value lie in the wavenumber range $16 \leqslant n \leqslant 40$. We can conclude that for the enstrophy flux criterion, the wavenumber range $16 \leqslant n \leqslant 40$ was the inertial subrange. The maximum value of the mixed stationary–transient flux of enstrophy was less than the maximum value for the transient flux. The former was nearly one half of the latter.

The enstrophy fluxes for the lower and upper troposphere were added to obtain

the flux distributions for the entire troposphere. A comparison of the enstrophy flux obtained by us for a summer month (July 1979) and the results of Shepherd (1987) for a winter month (January 1979) indicates that the transient and total fluxes were close to each other. Although the stationary fluxes were small, they were systematically down the scale in the summer while in winter the stationary fluxes were up the scale throughout the resolved scales. A comparison of enstrophy flux at 700(200) hPa with the flux in the lower (upper) troposphere once again confirmed that 700 hPa was a good representative level for the lower troposphere. But, this was not so for 200 hPa for the upper troposphere [figures 8(a) and (b)].

The spectra of available potential energy flux in the lower and upper troposphere are shown in figures 9(a) and (b). We find that all fluxes were down the scale throughout the wavenumber range $0 \leqslant n \leqslant 42$. The maximum available potential energy flux in the lower troposphere was twice its maximum value in the upper troposphere. The transient and stationary fluxes were one order less than the total flux. In the upper

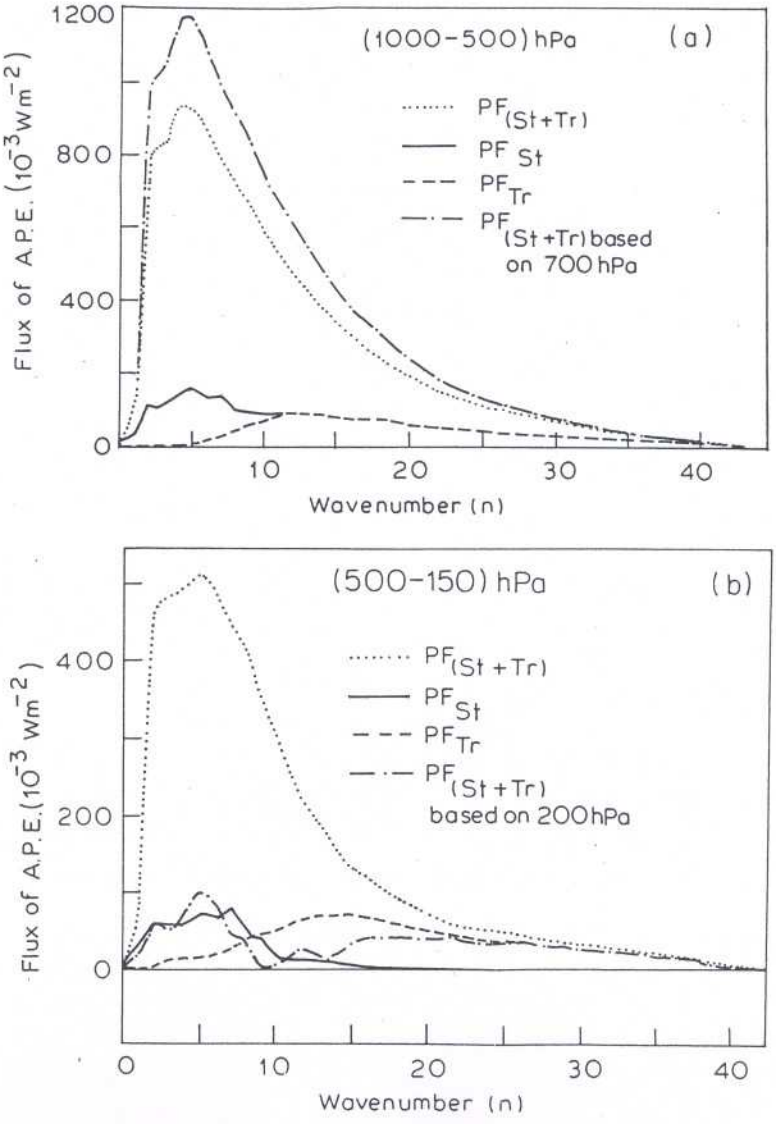


**Figure 9.** (a) and (b) are same as figures 7(a) and (b) for available potential energy.

troposphere the stationary flux was mainly confined to the low wavenumbers $n < 10$. But in the lower troposphere the flux penetrated upto wavenumber $n = 20$ with relatively stronger flux located at low wavenumbers. The transient flux was comparable to the stationary flux but larger values were confined to the wavenumber range $10 \leqslant n \leqslant 20$. A comparison of total flux with the transient and stationary flux indicated that the mixed stationary–transient flux dominates over the transient and stationary fluxes in the wavenumber domain $0 \leqslant n \leqslant 15$. We may conclude that the mixed stationary–transient interaction was stronger, comparable and weak compared to the transient–transient interactions for available potential energy, kinetic energy and enstrophy. For the flux of *APE*, 700 hPa and 200 hPa were not the satisfactory representative levels for the lower and upper troposphere. The same conclusion has been arrived on the basis of computed slopes.

## 5. Conclusions

- We have found that transient spectra of energy and enstrophy exhibit slopes which were less than the theoretical values for homogeneous isotropic turbulence. The departures from the theoretical slopes were less in the upper troposphere. The computed slopes of transient kinetic energy and enstrophy were closest to the theoretical value at 150 hPa. For *APE* this was at 400 hPa. In view of this, we conclude that dynamically the motion at 150 hPa was close to the homogeneous isotropic turbulence, while thermodynamically it was at 400 hPa. The change in slopes due to inclusion of the stationary component was relatively small because the stationary motion was weak compared to the transient motion in wavenumber range $14 \leqslant n \leqslant 25$.
- The spectral distribution of energy and enstrophy fluxes have shown that it was difficult to identify the inertial subrange for two dimensional wavenumber ($n$) without considering the contributions from the unresolved scales. The wavenumber range $14 \leqslant n \leqslant 25$ was close to the inertial subrange. The weak stationary fluxes of energy and enstrophy compared to their transient components suggest that the stationary nonlinear interactions may be neglected in comparison with transient and combined nonlinear interactions. Further, we find that the relative strength of stationary–transient component of flux with respect to its transient component was proportional to the relative strength of stationary component of energy and enstrophy with respect to its transient component.
- It may be concluded that the 700 hPa level can be used to a good approximation for studies of global energy and enstrophy spectra and their spectral fluxes in the lower troposphere during summer. For the upper troposphere the rough representative level was 200 hPa.

**Acknowledgements**

The authors are thankful to Shri D R Sikka, Director, IITM, Pune, for his interest in this study. The reanalysed FGGE-IIIb level data used in the study were obtained from European Centre for Medium Range Weather Forecasting, U.K.

## References

Baer F 1972 An alternate scale representation of atmospheric energy spectra; *J. Atmos. Sci.* **29** 649–664

Baer F 1974 Hemispheric spectral statistics of available potential energy; *J. Atmos. Sci.* **31** 932–941

Boer G J and Shepherd T G 1983 Large-scale two-dimensional turbulence in the atmosphere; *J. Atmos. Sci.* **40** 164–184

Charney J G 1971 Geostrophic turbulence; *J. Atmos. Sci.* **28** 1087–1095

Chen T C and Wiin-Nielsen A 1978 On nonlinear cascades of atmospheric energy and enstrophy in a two-dimensional spectral index; *Tellus* **30** 313–322

Eliasen E B, Machenhauer B and Rasmussen E 1970 On a numerical method for integration of the hydrodynamical equations with a spectral representation of the horizontal fields; *Rept No 2 Inst. Theor. Meteor. Copenhagen University* **35**

Fjortoft R 1953 On the changes in spectral distribution of kinetic energy for two-dimensional, nondivergent flow; *Tellus* **5** 225–230

Gates W L 1961 Static stability measures in the atmosphere; *J. Meteorol.* **18** 526–533

Kraichnan R H 1967 Inertial subranges in two-dimensional turbulence; *Phys. Fluids* **10** 1417–1423

Lambert S J 1984 A global available potential energy-kinetic energy budget in terms of the two-dimensional wavenumber for the FGGE year; *Atmosphere-Ocean* **22** 265–282

Leith C E 1968 Diffusion approximation for two-dimensional turbulence; *Phys. Fluids* **11** 671–673

Leith C E 1971 Atmospheric predictability and two-dimensional turbulence; *J. Atmos. Sci.* **28** 145–161

Lesieur M 1987 *Turbulence in fluids* (eds) R J Moreau and G A Oravas, (The Netherlands: Martinus Nijhoff Publishers) pp. 187

Merilees P E 1979 On the kinematic properties of the $-3$ law for kinetic energy; *Tellus* **31** 487–492

Robert A J 1966 The integration of a low order spectral form of the primitive meteorological equation; *J. Meteorol. Soc. Jpn.* **44** 237–245

Shepherd T G 1987 A spectral view of nonlinear fluxes and stationary–transient interaction in the atmosphere; *J. Atmos. Sci.* **44** 1166–1178